Numerical Heat Transfer, Part A: Applications

An International Journal of Computation and Methodology

ISSN: 1040-7782 (Print) 1521-0634 (Online) Journal homepage: http://www.tandfonline.com/loi/unht20

Turbulent Heat Transfer Analysis of a Three-Dimensional Array of Perforated Fins Due to Changes in Perforation Sizes

Mohammad Reza Shaeri & Tien-Chien Jen

To cite this article: Mohammad Reza Shaeri & Tien-Chien Jen (2012) Turbulent Heat Transfer Analysis of a Three-Dimensional Array of Perforated Fins Due to Changes in Perforation Sizes, Numerical Heat Transfer, Part A: Applications, 61:11, 807-822

To link to this article: http://dx.doi.org/10.1080/10407782.2012.671046

Published online: 07 Jun 2012.

Numerical Heat Transfer, Part A, 61: 807–822, 2012

ISSN: 1040-7782 print/1521-0634 online
DOI: 10.1080/10407782.2012.671046

Taylor & Francis
Taylor & Francis Group

TURBULENT HEAT TRANSFER ANALYSIS OF A THREE-DIMENSIONAL ARRAY OF PERFORATED FINS DUE TO CHANGES IN PERFORATION SIZES

Mohammad Reza Shaeri and Tien-Chien Jen
Department of Mechanical Engineering, University of Wisconsin-Milwaukee, Milwaukee, Wisconsin, USA

Turbulent heat transfer characteristics of three-dimensional and rectangular perforated fins, including perforation like channels along the length of the fins, are investigated. Both dimensions and numbers of perforations are changed at the highest porosity in the study of Shaeri and Yaghoubi [7] to determine the effects of perforation sizes on the heat transfer characteristics of the perforated fins. Results show that at a specific porosity, a fin with a higher number of perforations enhances the heat transfer rate more efficiently. Also, total drag is not only remarkably lower in perforated fins compared with a solid fin, but also becomes smaller by decreasing the number of perforations.

1. INTRODUCTION

The wide industrial applications of extended surfaces, or fins, to enhance the heat transfer rate highlight the need for further research in the performance and optimization of fins. Among all fin types, rectangular fins are commonly used due to simplicity in manufacturing [1]. Dogan and Sivrioglu [2] considered a broad range of Reynolds numbers and experimentally studied mixed convection heat transfer from longitudinal fins for different fin heights and spaces. Yalcin et al. [3] investigated the effect of fin geometry on convection heat transfer from an array of rectangular fins. Didarul et al. [4] experimentally studied the effects of fin height, inclination angle, fin pattern, and Reynolds number on flow and heat transfer characteristics of short, rectangular plate fins. For thermal diffusion in a fin with a rectangular profile, Moitsheki [5] proposed several exact solutions while the thermal conductivity and heat transfer coefficient were considered temperature-dependent. Youcef-Ali and Desmons [6] developed a mathematical model to predict thermal performance of a solar collector that was equipped with a rectangular plate fin. Other studies related to rectangular fins are found in references [7–13].

Received 30 September 2011; accepted 10 February 2012.
The authors gratefully acknowledge Professor Hajime Nakamura in the Department of Mechanical Engineering, National Defense Academy, Hashirimizu, Yokosuka, Japanfor providing us with the experimental data.

Address correspondence to Tien-Chien Jen, Department of Mechanical Engineering, University of Wisconsin-Milwaukee, Milwaukee, WI-53211, USA. E-mail: jent@uwm.edu

NOMENCLATURE

ΔA	area (m^2)
A_F	fin area that is touched by air in flow direction, m^2
A_P	frontal area of fin, m^2
A_D	reference area to calculate the average drag coefficient, m^2
$\overline{C_D}$	average drag coefficient
C_p	specific heat at constant pressure, $J \cdot Kg^{-1} \cdot K^{-1}$
D, H, L, S_f	fin thickness, height, length and spacing, respectively, m
F_F, F_P, F_D	friction, pressure and total drag, respectively, N
Gr	Grashof number
$h, \bar{h}$	local and average convection heat transfer coefficient, respectively, $W \cdot m^{-2} \cdot K^{-1}$
H_d	block height in reference [36], m
H_p, W_p	perforation height and width, respectively, m
k	turbulent kinetic energy, $m^2 \cdot s^{-2}$
N	number of perforation
$Nu_L, \overline{Nu}_L$	local and average Nusselt numbers, respectively, based on the fin length
P	air pressure, Pa
$\dot{Q}$	heat dissipation rate from the fin, W
Re	Reynolds number, $\left(\frac{\rho u_\infty H_d}{\mu}\right)$
Re_L	Reynolds number based on the fin length, $\left(\frac{\rho u_\infty L}{\mu}\right)$
T	temperature, K
u, v, w	velocity components in X, Y, and Z directions, respectively, $m \cdot s^{-1}$
X, Y, Z	rectangular coordinates
Subscripts	
b	fin base
DS, US	downstream and upstream, respectively
in	inlet
S	surface of the fin
∞	free stream
δ	turbulent boundary layer in reference [36]
ε	turbulent dissipation rate, $m^2 \cdot s^{-3}$
ε_f	fin effectiveness
μ, μ_t	laminar and turbulent air viscosity, respectively, $Kg \cdot m^{-1} \cdot s^{-1}$
ρ	air density, $Kg \cdot m^{-3}$
λ, λ_t	laminar and turbulent thermal conductivity of fluid, respectively, $W \cdot m^{-1} \cdot K^{-1}$
Φ	porosity
τ_w	wall shear stress, Pa

Generally, fin optimization is categorized in two groups: 1) reducing the weight of a fin at a given amount of heat transfer rate, and 2) increasing the rate of heat transfer at a given fin weight [14]. Studies on fin optimization are extensive. Kim and Kuznetsov [15] numerically optimized thermal performance of anisotropic pin-fin heat sink. They reported that thickness and height of the pin-fin, as well as the Reynolds number, are the major parameters to determine the optimum porosity for maximum heat transfer. In their study, a correlation to predict the optimum porosity was proposed, as well. Karvinen and Karvinen [16] proposed a method to find the geometry of a plate fin to maximize the heat dissipation in both forced and natural convection. Kim et al. [17] investigated thermal optimization of a heat sink, including plate-fins by focusing on change in fin thickness. Park et al. [18] investigated the optimization of the shape and arrangement of a plate heat exchanger including staggered pin arrays. Other fin optimization studies are found in references [9, 10, 19–22].

The use of perforated fins is one of the most prevalent methods in fin optimization, since they may enhance the heat transfer rate and certainly reduce fin weight; therefore, two fin optimization goals can be simultaneously achieved. According to reference [23], while a simple solid baffle plate attached to the duct wall enhances

heat transfer, a perforated plate attached to the same duct wall poses less resistance to the flow and thus might have a better performance.

Investigating the heat transfer characteristics of heat exchangers equipped with square cross–sectional perforated pin fins was performed in an experimental study by Sahin and Demir [24]. Sara et al. [25] used perforated blocks with rectangular cross-sections to study the heat transfer enhancement from a flat surface. Dorignac et al. [26] experimentally determined convective heat transfer from a multi-perforated plate and proposed an empirical correlation for heat exchange at the windward surface of a perforated flat plate for a wide range of perforation spacings. Shaeri et al. [1] and Yaghoubi et al. [27] numerically studied the fluid flow and heat transfer around a three-dimensional, longitudinal, and rectangular array of perforated fins in turbulent and laminar flow, respectively. In their studies, perforations like windows in various numbers and sizes were placed in the lateral surfaces of the fins. They reported that by using these types of perforated fins, one can obtain fins that are 65% lighter with no loss in the heat transfer ratecompared with solid fins.

Shaeri and Yaghoubi [7, 8] numerically investigated the three-dimensional turbulent and laminar heat transfer characteristics of an array of longitudinal and rectangular perforated fins with perforation-like channels placed along the length of fins. By using perforated fins in references [7, 8], a significant increase in the heat transfer rate, especially in turbulent flow, and a significant decrease in solid fin weight were reported. Furthermore, Shaeri and Yaghoubi [7] defined porosity as the ratio of the volume occupied by the perforations (empty volume) to the total volume of the solid fin (fin without perforation) and focused on heat transfer characteristics at different porosities. They reported that a fin with higher porosity enhances the heat transfer rate more efficiently. Furthermore, their study also demonstrated that fins with three perforations enhanced the heat transfer rate by almost twice as that of the solid fin, and reduced the weight of the solid fin by more than 56%.

The aim of the present study is to investigate the effects of changes in the sizes and the number of perforations on the turbulent heat transfer characteristics of the fin with the highest porosity in reference [7]. In other words, the fin with three perforations in reference [7] is selected and its sizes and numbers of perforations change while its porosity remains unchanged. For a complete comparison, all the operating conditions in this study are exactly the same as those in reference [7]. Results include comparisons of friction and pressure drags, as well as Nusselt number and heat transfer performances of the perforated fins at different Reynolds numbers in turbulent flow.

2. PROBLEM DESCRIPTION

Figure 1 illustrates the fin array configurations and their cross-sections. The fin in Figure 1*d* has the highest perforations (porosity) and heat transfer enhancement in reference [7]. The fins in Figures 1*b* and 1*c* are at the same porosity as that of the fin in Figure 1*d*, but differ in the number and size of perforations. Table 1 provides details about the perforated fins investigated in this study.

The steady-state airflow with constant thermal and flow properties with inlet velocity u_∞ contacts the faces of the fins and inside the perforations. For the fins shown in Figure 1, the velocity of air varies in such a manner that the Reynolds

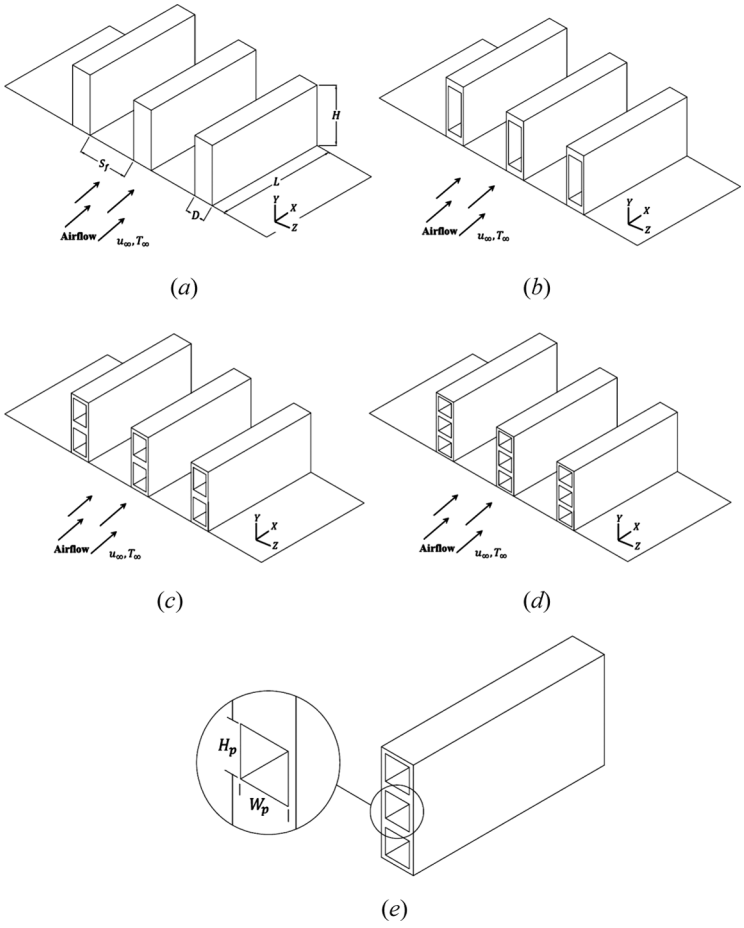

Figure 1. Configurations of fin arrays at the present study. (*a*) An array of solid fins; (*b*) an array of fins with one perforation; (*c*) an array of fins with two perforations; (*d*) an array of fins with three perforations; and (*e*) cross-section of perforations.

number based on the fin length Re_L is in the range of $2 \times 10^4 - 4 \times 10^4$. At this range, flow inside the perforations (ducts) remains turbulent so that the Reynolds number based on the hydraulic diameter of perforations ranges 3,750–7,500, 3,000–6,000 and

Table 1. Geometries of various types of fins in turbulent flow

Number of perforation, N	Fin length, L (mm)	Fin height, H (mm)	Fin thickness, D (mm)	Fin spacing, S_f (mm)	Perforation width, W_p (mm)	Perforation height, H_p (mm)	Porosity (ϕ)
0	24	12	4	10	0	0	0
1	24	12	4	10	3	9	0.56
2	24	12	4	10	3	4.5	0.56
3	24	12	4	10	3	3	0.56

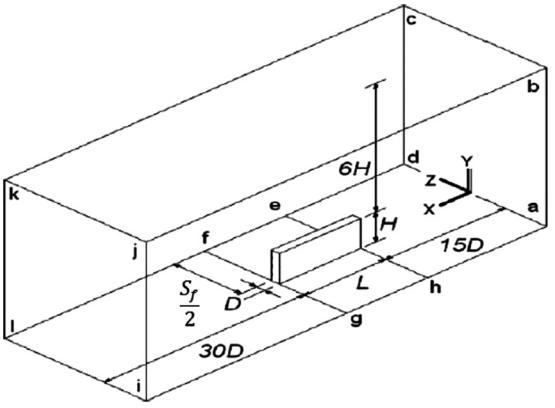

Figure 2. Computational domain for fins in Figure 1.

2,500–5,000 for array of fins in Figures 1*b*, 1*c*, and 1*d*, respectively. Also, the corresponding Richardson number $\left(\mathrm{Gr}/\mathrm{Re}^2\right)$ based on the fin height is less than 0.001, which shows the effect of free convection can be neglected appropriately. Aluminum with thermal conductivity of $202\,\mathrm{W}\cdot\mathrm{m}^{-1}\cdot\mathrm{K}^{-1}$ was chosen as the fin material, which is usual in fin construction.

Due to the uniform air flow and symmetry in the fin arrays, computations are applied just for one fin instead of the total array of fins [1, 7, 8, 27]. Figure 2 illustrates the computational domain that is exactly identical to that of reference [7]. As two of the most important parameters in a numerical simulation, upstream and downstream distances were chosen by some tests, taking advantage of previous studies such as [1, 7, 8, 27, 28]. In Figure 2, plane abcd is the inlet boundary and a uniform flow condition is considered for all variables using $u_{in}=u_\infty$, $v_{in}=w_{in}=0$, and $T_{in}=T_\infty=25^\circ\mathrm{C}$. In addition, similar conditions were applied for plane bckj as the free stream plane. For plane ijkl, which is the outlet plane and is far enough from the fin, zero gradient of variables in X direction, $\frac{\partial u}{\partial X}=0$ was applied. Planes abji and dckl are symmetry planes; therefore, the conditions of zero gradients in Z direction, $\frac{\partial u}{\partial Z}=0$ and $w=0$ were dictated in these planes. The remaining planes are wall with no-slip boundary condition. Plane efgh as the fin base has a constant temperature equal to 70°C and planes adeh and gfli were assumed adiabatic. According to reference [29], the radiation heat transfer rate is less than 5% and 8% of the total heat transfer rate for polished aluminum fins with temperature differences around 40°C and 77.5°C, respectively. Therefore, since the maximum temperature difference in this study is 45°C, the effect of radiation heat transfer rate is ignored.

3. GOVERNING EQUATIONS

The governing equations for three-dimensional and incompressible steady-state turbulent flow are described as follows.

Continuity equation

$$\frac{\partial u_i}{\partial X_i} = 0 \tag{1}$$

Momentum equation

$$\frac{\partial}{\partial X_j}(\rho u_i u_j - \tau_{ij}) = -\frac{\partial P}{\partial X_i} \tag{2}$$

Stress equation

$$\tau_{ij} = 2\mu S_{ij} - \frac{2}{3}\mu_t \frac{\partial u_k}{\partial X_k}\delta_{ij} \tag{3}$$

Turbulent viscosity

$$\mu_t = \frac{\rho C_\mu k^2}{\varepsilon} \tag{4}$$

The distortion rate tensor S_{ij} and the Kronecker delta function δ_{ij} can be written as follows.

$$S_{ij} = \frac{1}{2}\left(\frac{\partial u_i}{\partial X_j} + \frac{\partial u_j}{\partial X_i}\right) \tag{5}$$

$$\delta_{ij} = \begin{cases} 1, & i = j \\ 0, & i \neq j \end{cases} \tag{6}$$

Energy equation

$$\rho C_p \frac{\partial(u_i T)}{\partial X_i} = \frac{\partial}{\partial X_i}\left[\frac{\partial T}{\partial X_i}(\lambda + \lambda_t)\right] \tag{7}$$

The effects of rapid strain and streamline curvature, flow separation, reattachment, and recirculation can be modeled better by the RNG turbulent modeling rather than the standard k–ε model [28]. The use of RNG k–ε modeling can be found in several investigations such as references [1, 7, 28, 30–33]. Yakhot et al. [34] proposed a variant of the k–ε model such that its performance characteristics improved relative to the standard model as follows [1].

Turbulent kinetic energy equation

$$\frac{\partial(\rho u_i k)}{\partial X_i} = \frac{\partial}{\partial X_i}\left[\alpha_k \mu_{eff} \frac{\partial k}{\partial X_i}\right] + \mu_t S^2 - \rho\varepsilon \tag{8}$$

Turbulent energy dissipation rate

$$\frac{\partial(\rho u_i \varepsilon)}{\partial X_i} = \frac{\partial}{\partial X_i}\left[\alpha_\varepsilon \mu_{eff} \frac{\partial \varepsilon}{\partial X_i}\right] + C_{1\varepsilon}\mu_t S^2 \frac{\varepsilon}{k} - C^*_{2\varepsilon}\rho\frac{\varepsilon^2}{k} \tag{9}$$

where the effective viscosity μ_{eff} and the mean rate of strain tensor S are defined as $\mu_{eff} = \mu + \mu_t$ and $S = \sqrt{2S_{ij}S_{ij}}$, respectively. $C^*_{2\varepsilon}$ contains the additional source; that is, the main difference between the RNG k–ε and the standard k–ε turbulent models. Although $C^*_{2\varepsilon}$ is constant in a standard k–ε model, it takes the following form in the RNG model.

$$C^*_{2\varepsilon} = C_{2\varepsilon} + \frac{C_\mu \eta^3\left(1 - \frac{\eta}{\eta_0}\right)}{1 + \beta\eta^3} \tag{10}$$

where $\eta = Sk/\varepsilon$, $\eta_0 = 4.38$, $\beta = 0.012$ [34]. The other experimental constants in the above equations are as follows: and $\alpha_k = \alpha_\varepsilon = 1.393$, $C_{1\varepsilon} = 1.42$, $C_{2\varepsilon} = 1.68$, and $C_\mu = 0.0845$.

4. COMPUTATIONAL METHOD

4.1. Grid Generation

As one of the most important steps in numerical simulation, grid points must be generated precisely to obtain correct flow and temperature characteristics in the computational domain. For proper prediction of the recirculation zone and the reattachment point, the grid points should be dense near the solid faces [7]. Moreover, the solution must be independent of the number of grid points; therefore, for each fin the number of grid points in three dimensions in the computational domain increases until an independency in solution is achieved. As an example, Table 2 shows a grid study procedure for the fin presented in Figure 1*b*.

Based on the results provided in Table 2, for denser grids compared with those in step 4, the changes of average Nusselt numbers and total drags in flow direction are less than 2.1% and 1.2%, respectively. Therefore, by increasing the number of grid points in step 4, the marked difference in flow characteristics will not be obtained. Therefore, to compute faster and to save computer memory, the number

Table 2. Grid independent study for fin with 1 perforation at $\mathrm{Re}_L = 2.5 \times 10^4$

Step	Number of grids in whole domain, (X, Y, Z)	Average Nusselt number, $\overline{Nu_L}$	Total drag in flow direction, (N)
1	$100 \times 46 \times 31$	127.16	4.656×10^{-3}
2	$150 \times 70 \times 48$	133.49	5.050×10^{-3}
3	$175 \times 82 \times 54$	134.88	5.199×10^{-3}
4	$200 \times 101 \times 61$	139.75	5.223×10^{-3}
5	$230 \times 116 \times 79$	140.75	5.246×10^{-3}
6	$250 \times 134 \times 87$	142.63	5.285×10^{-3}

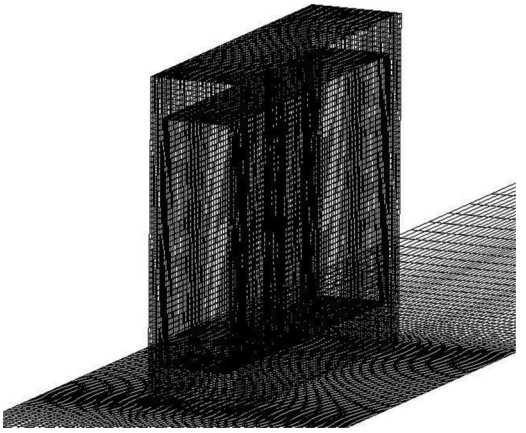

Figure 3. Grid structure for fin with one perforation.

of grid points equal to $200 \times 101 \times 61$ are selected to analyze the turbulent flow and heat transfer for a fin with one perforation. The same process has been performed for other fins, and a suitable number of grid points have been adopted for them. The final grid structure for the fin in Figure 1*b* is shown in Figure 3.

4.2. Computational Procedure

Similar to reference [7], the governing equations are discretized using a finite volume code and the QUICK technique [35], and solved using the SIMPLE algorithm [35]. The set of discretized equations has been solved iteratively with the line-by-line method. Computations began by first solving the continuity, momentum, k, and ε equations to determine the flow field and then the energy equation to find the thermal field in the computational domain.

In reference [35], the final discretized equation for a computational cell p is considered as the follows.

$$a_p \varphi_p = \sum (a_{nb} \varphi_{nb}) + b \tag{11}$$

where φ_p is the property of the computational cell p that is needed to be calculated, such as velocity, temperature, etc. The indices nb refer to the neighboring computational cells of the cell p. Also, the factor a represents the coefficient of the property at the computational cell, and b relates to the source term that obtained after discretization of equations. Each set of equations will be solved until the following convergence criterion is satisfied.

$$R = \frac{\sum_1^N |\sum (a_{nb} \varphi_{nb}) + b - a_p \varphi_p|}{\sum_1^N |a_p \varphi_p|} \tag{12}$$

where R is the residual. Note, that Eq. (12) is applied for all the computational cells in the computational domain. N, the upper bound of summation, shows the total number of computational cells in the domain.

However, the convergence criterion for the continuity equation is considered as follows.

$$R = \frac{\sum_1^N |\text{rate of mass accumulation in cell } i|}{N} \tag{13}$$

where N is the total number of computational cells.

In the present study, the minimum convergence criterion for continuity and other equations are considered $1 \times 10^{-6}$and 1×10^{-8}, respectively.

5. VALIDATION

This study uses the same numerical code as in reference [7] to compare the turbulent heat transfer characteristics of the fins in this investigation with those with the highest porosity in reference [7]. The numerical code in reference [7] was validated with an experiment and a good agreement was obtained between the simulation and the experiment. For more confidence, the numerical code at this study was compared again with other experimental results. Since there is no experimental study regarding the perforated fins similar to the fins used in this study, the simulated heat transfer characteristics of the solid fin are compared with those obtained by an experiment.

Nakamura et al. [36] experimentally investigated the turbulent fluid flow and local heat transfer around a cube mounted on a wall under constant heat flux, and proposed a relation to predict the overall Nusselt number for the cube. They performed the experiment in a wind tunnel, with its height, width, and length equal to 400 mm, 300 mm and 800 mm, respectively, and placed a cube 30 mm in height on the floor of the wind tunnel [36]. In their study, the Reynolds number was defined based on the cube height and changed from 4.2×10^3 to 3.3×10^4; therefore, the free-stream velocity was in the range of $2.2\,\text{m} \cdot \text{s}^{-1}$ to $17.3\,\text{m} \cdot \text{s}^{-1}$. The turbulent boundary layer δ was 1.5–1.83 times larger than the cube height in the experiment. The same condition was simulated in this study to validate the results of the numerical investigation with those obtained from the experiment in reference [36]. Figure 4 illustrates the obtained values of the overall Nusselt numbers at different Reynolds numbers for a wall-mounted cube from both experiments in reference [36] and the current simulation.

According to Figure 4, the good agreement between the results obtained from the present simulation and the experiment in reference [36] proves the accuracy of the numerical code in this study.

6. RESULTS AND DISCUSSIONS

The flow field and convection heat transfer has been studied in the range of $\text{Re}_L = 2 \times 10^4 - 4 \times 10^4$ for an array of perforated fins in turbulent flow. It is evident that because of perforations, some part of the flow enters them, and for this reason

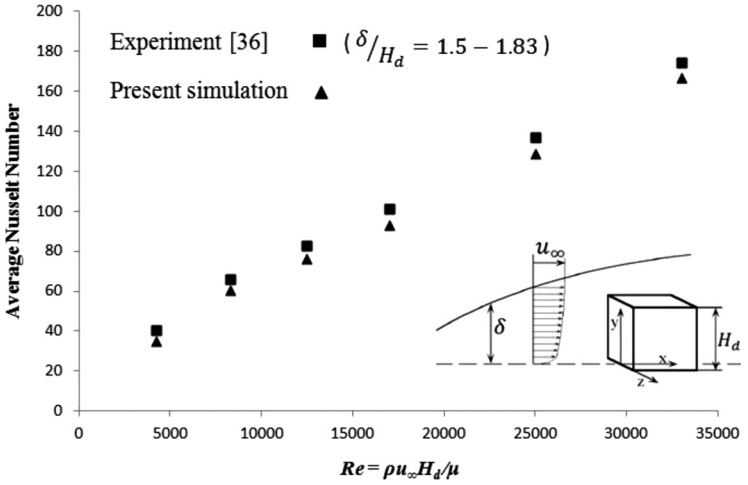

Figure 4. Comparison of numerical and experimental average Nusselt numbers around a block. (This figure is produced by permission of the publisher of reference [36].)

the drag force that acts on the faces of perforated fins differs from that of acting on the surfaces of a solid fin. The drag force has two components: 1) friction drag due to the surface shear stress; and 2) pressure drag due to the pressure difference in flow direction. Friction, pressure, total drags, and the average drag coefficient are calculated through Eqs. (14)–(17) [1, 7].

$$F_F = \sum_{i}^{(\tau_w)} \Delta A_i = \sum^{\mu} \left(\frac{\partial u}{\partial n_i}\right) \Delta A_i \tag{14}$$

$$F_P = \left(-\sum_{i}^{P} \Delta A_i\right)_{US} - \left(-\sum_{i}^{P} \Delta A_i\right)_{DS} \tag{15}$$

$$F_D = F_F + F_P \tag{16}$$

$$\overline{C_D} = \frac{F_D}{\frac{1}{2} A_D \rho u_\infty^2} \tag{17}$$

where in Eq. (14), τ_w is the wall shear stress over the faces of fins, including outer walls of the fins and inner walls of the perforations. Note, that in Eq. (14) the area is equal to the total fin area that is touched by the air in the flow direction, as follows [7].

$$A_F = 2H \times L + D \times L + 2N \times L \times H_P + 2N \times L \times W_P \tag{18}$$

In Eq. (15), the area relates to the area in front and back of the solid part (frontal area) of the fin that is perpendicular to the flow stream, given as [7] follows.

$$A_P = D \times H - N \times H_P \times W_P \tag{19}$$

To compare the average drag coefficients of different fins, a unique reference area A_D that is equal among all types of fins is introduced and used in Eq. (17) [7]. This reference area is equal to the sum of the areas of lateral surfaces and top surface of the fins and is given by the following relation [7].

$$A_D = 2L \times H + L \times D \tag{20}$$

Figure 5 illustrates the variations of friction, pressure and total drags, as well as theaverage drag coefficient.

Note, that the flow around arrays of solid fins in turbulent flow becomes unsteady from $\mathrm{Re}_L = 25 \times 10^3$ onwards [7]; therefore, the results of the solid fin are shown only in the range of $\mathrm{Re}_L = 20 \times 10^3 - 25 \times 10^3$.

It is evident that the fin area touched by fluid is higher in perforated fins compared with solid fins; therefore, friction drag in a perforated fin should be higher than that of a solid fin. Moreover, the area of the fin touched by fluid increased by adding the number of perforations due to the increase in the ceilings and floors

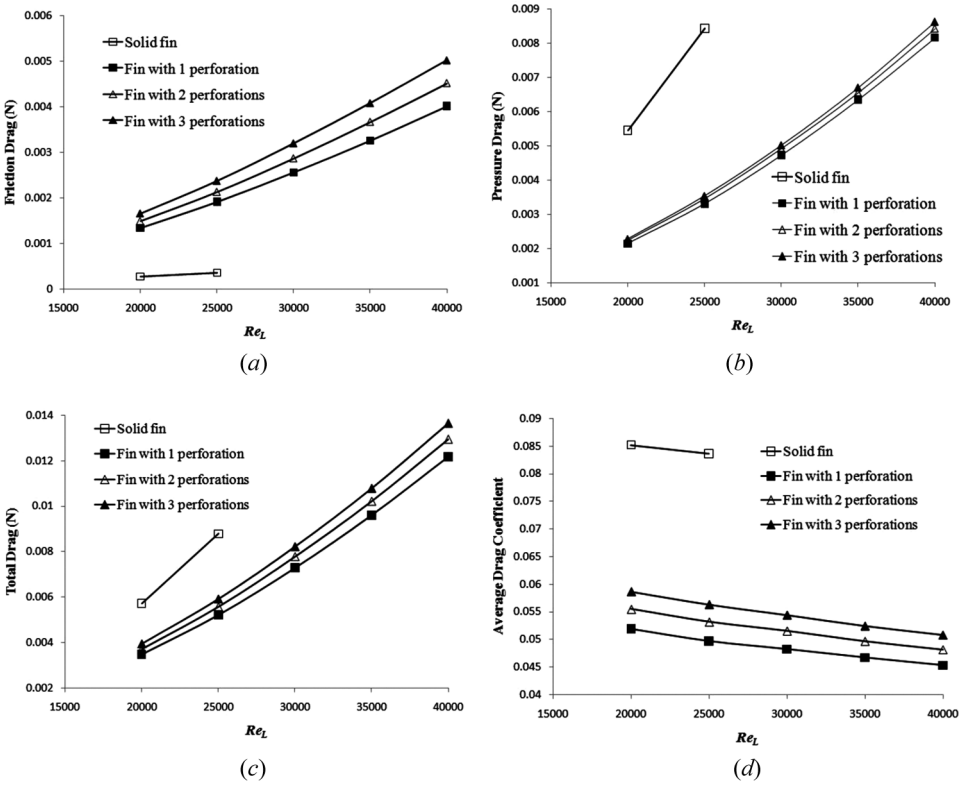

Figure 5. (*a*) Variation of friction drag in flow direction for various types of fins; (*b*) variation of pressure drag in flow direction for various types of fins; (*c*) variation of total drag in flow direction for various types of fins; and (*d*) variation of average drag coefficient in flow direction for various types of fins.

of extra perforations; therefore, friction drag becomes larger due to the increase in the number of perforations.

However, the frontal area is maximum in the solid fin and the same among perforated fins; therefore, a higher pressure drag for the solid fin and almost the same pressure drag among the perforated fins can be expected. Note, that the small difference in pressure drag among perforated fins can be due to the configuration and location of the perforations. Based on Figure 5*b*, a decrease in the number of perforations causes the pressure drag to go down negligibly. According to Figures 5*c* and 5*d*, total drag is remarkably higher for the solid fin and becomes smaller slightly by decreasing the number of perforations (increase in the perforation sizes). Therefore, at a specific porosity, one can significantly reduce total drag using perforated fins with a lower number of perforations.

The Nusselt number, the given nondimensional parameter in Eq. (21), has an important role to predict the heat transfer characteristics of an object.

$$\mathrm{Nu}_L = \frac{hL}{\lambda} \tag{21}$$

Figure 6 illustrates and compares the local distribution of Nusselt number in flow direction at the inner surface of the fins with one and two perforations.

According to Figure 6, thermal entrance lengths of both perforations in the fin with two perforations are almost the same and nearly equal to that of the fin with

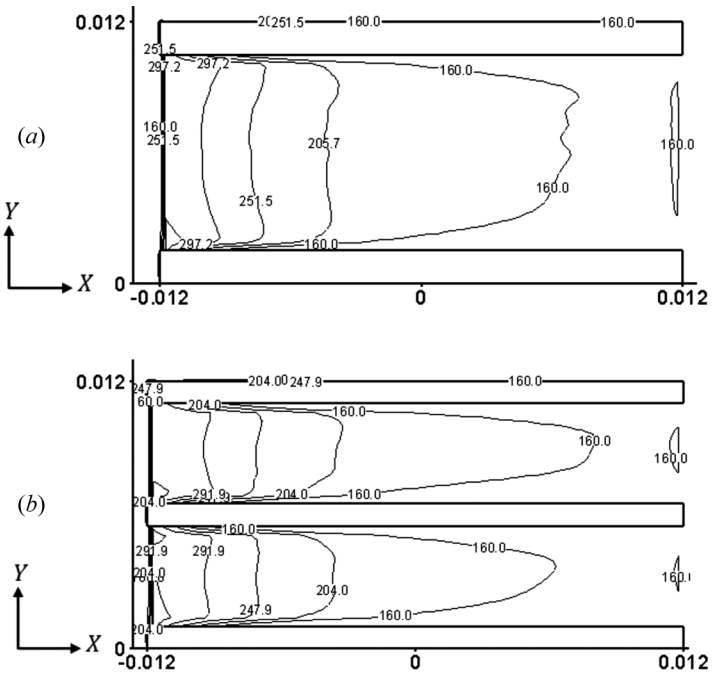

Figure 6. Distribution of the local Nusselt number in flow direction at $\mathrm{Re}_L = 4 \times 10^3$ for perforated fins with (*a*) one perforation and (*b*) two perforations.

one perforation; therefore, it is expected that the heat transfer rates from all perforations are almost the same, and the heat transfer rate increases by using fins with more perforations.

Fin effectiveness, as a nondimensional parameter, is representative of the performance of a fin [37], and defined as the ratio of the heat transfer rate by the fin to the heat transfer rate from the base of the fin, when the base is not equipped with the fin. The following relation mathematically describes the fin's effectiveness.

$$\varepsilon_f = \frac{\dot{Q}}{\overline{h}_b A_b (T_b - T_\infty)} \tag{22}$$

where $\dot{Q}$ is the heat dissipation rate from the fin, which can be calculated by the following relation [7].

$$\dot{Q} = \sum h_i \Delta A_i (T_S - T_\infty) \tag{23}$$

Figure 7 illustrates the heat transfer performances of varied kinds of fins at different Reynolds numbers.

Based on Figure 7, a significant increase in the heat transfer rate can be obtained by using perforated fins, and this advantage is fully explained in reference [7]. Also, at a specific porosity, adding the number of perforations (reducing the size of perforations) increases the heat transfer rate in a turbulent flow in such a manner that a fin with three perforations enhances the heat transfer rate the most. This conclusion completely agrees with the variation of local Nusselt numbers shown in Figure 6.

Moreover, by using the proposed perforated fins in the present study much lighter fins will be obtained, reducing the weight of the solid fin by nearly 56%. Consequently, using the presented types of perforated fins enables two fin optimization

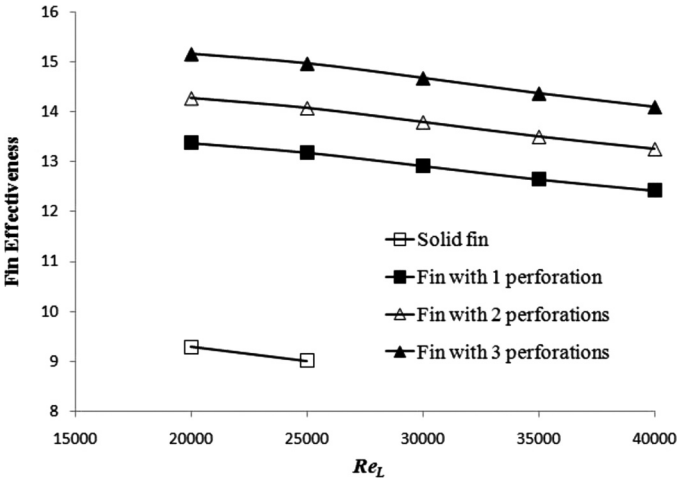

Figure 7. Variation of fin effectiveness at different Reynolds numbers.

goals to be met. Therefore, it can be concluded that regardless of difficulties in manufacturing the proposed perforated fins, they are economical in saving the primary material of the fins [7, 8].

7. CONCLUSIONS

A supplemental study of reference [7] was performed to investigate the effects of the number of perforations and their sizes on the turbulent heat transfer characteristics of the perforated fins. It was shown in reference [7] that fins with perforations along the length increase the heat transfer rate much more efficiently; therefore, the most efficient perforated fin in reference [7] was selected and its heat transfer characteristics were compared with those of the perforated fins at the same porosity, but at different perforation sizes and numbers in the present study. The results include the following.

- Due to a larger fin area touched by the fluid, a perforated fin has a higher friction drag compared with a solid fin. Friction drag is also higher for fins with more perforations due to an increase in the floors and the ceilings of the extra perforations.
- Since the frontal area A_P is higher in a solid fin, pressure drag is much higher for a solid fin compared with perforated fins. Due to the same frontal area for all the perforated fins, a marked difference cannot be observed in pressure drag among different perforated fins.
- Perforated fins reduce the total drag significantly, and the total drag becomes smaller by decreasing the number of perforations (increasing the size of perforations).
- The proposed perforated fins in this study significantly enhance the heat transfer rate. Also, at the same porosity the heat transfer rate becomes larger due to the increase in the number of perforations (reducing the perforation sizes).
- Using the perforated fins in this study can greatly reduce the weight of a solid fin. Consequently, both goals of fin optimization can be achieved by applying these types of perforated fins.

REFERENCES

1. M. R. Shaeri, M. Yaghoubi, and K. Jafarpur, Heat Transfer Analysis of Lateral Perforated Fin Heat Sinks, *Appl. Energy*, vol. 86, pp. 2019–2029, 2009.
2. M. Dogan and M. Sivrioglu, Experimental Investigation of Mixed Convection Heat Transfer from Longitudinal Fins in a Horizontal Rectangular Channel, *Int. J. Heat Mass Transfer*, vol. 53, pp. 2149–2158, 2010.
3. H. G. Yalcin, S. Baskaya, and M. Sivrioglu, Numerical Analysis of Natural Convection Heat Transfer from Rectangular Shrouded Fin Arrays on a Horizontal Surface, *Int. Comm. Heat Mass Transfer*, vol. 35, pp. 299–311, 2008.
4. I. M. Didarul, O. Kenyu, Y. Minoru, and S. Izuru, Study on Heat Transfer and Fluid Flow Characteristics with Short Rectangular Plate Fin of Different Pattern, *Experi. Therm. and Fluid Sci.*, vol. 31, pp. 367–379, 2007.
5. R. J. Moitsheki, Steady Heat Transfer through a Radial Fin with Rectangular and Hyperbolic Profiles, *Nonlinear Analysis: Real World Applications*, vol. 12, pp. 867–874, 2011.

6. S. Youcef-Ali and J. Y. Desmons, Numerical and Experimental Study of a Solar Equipped with Offset Rectangular Plate Fin Absorber Plate, *Renewable Energy*, vol. 31, pp. 2063–2075, 2006.
7. M. R. Shaeri and M. Yaghoubi, Numerical Analysis of Turbulent Convection Heat Transfer from an Array of Perforated Fins, *Int. J. Heat Fluid Flow*, vol. 30, pp. 218–228, 2009.
8. M. R. Shaeri and M. Yaghoubi, Thermal Enhancement from Heat Sinks by using Perforated Fins, *Energy Conversion and Management*, vol. 50, pp. 1264–1270, 2009.
9. A. Aziz and A. B. Beers-Green, Performance and Optimum Design of Convective–Radiative Rectangular Fin with Convective Base Heating, Wall Conduction Resistance, and Contact Resistance between the Wall and the Fin Base, *Energy Conversion and Management*, vol. 50, pp. 2622–2631, 2009.
10. X. Zhang and D. Liu, Optimum Geometric Arrangement of Vertical Rectangular Fin Arrays in Natural Convection, *Energy Conversion and Management*, vol. 51, pp. 2449–2456, 2010.
11. H. Jouhara and B. P. Axcell, Modelling and Simulation Techniques for Forced Convection Heat Transfer in Heat Sinks with Rectangular Fins, *Simulation Modelling Practice and Theory*, vol. 17, pp. 871–882, 2009.
12. S. Baskaya, M. Sivrioglu, and M. Ozek, Parametric Study of Natural Convection Heat Transfer from Horizontal Rectangular Fin Arrays, *Int. J. Therm. Sci.*, vol. 39, pp. 797–805, 2000
13. S. A. El-Sayed, S. M. Mohamed, A. A. Abdel-latif, and A.-H. E. Abouda, Experimental Study of Heat Transfer and Fluid Flow in Longitudinal Rectangular-Fin Array Located in Different Orientations in Fluid Flow, *Exper. Therm. and Fluid Sci.*, vol. 29, pp. 113–128, 2004.
14. C. Arslanturk and A. F. Ozguc, Optimization of a Central-Heating Radiator, *Appl. Energy*, vol. 83, pp. 1190–1197, 2006.
15. S. Y. Kim and A. V. Kuznetsov, Optimization of Pin-Fin Heat Sinks using Anisotropic Local Thermal Nonequilibrium Porous Model in a Jet Impinging Channel, *Numer. Heat Transfer A*, vol. 44, pp. 771–787, 2003.
16. R. Karvinen and T. Karvinen, Optimum Geometry of Fixed Volume Plate Fin for Maximizing Heat Transfer, *Int. J. Heat Mass Transfer*, vol. 53, pp. 5380–5385, 2010.
17. D.-K. Kim, J. Jung, and S. J. Kim, Thermal Optimization of Plate-Fin Heat Sinks with Variable Fin Thickness, *Int. J. Heat Mass Transfer*, vol. 53, pp. 5988–5995, 2010.
18. K. Park, D.-H. Choi, and K.-S. Lee, Optimum Design of Plate Heat Exchanger with Staggered Pin Arrays, *Numer. Heat Transfer A*, vol. 45, pp. 347–361, 2004.
19. M.-S. Kim, J. Lee, S.-J. Yook, and K.-S. Lee, Correlations and Optimization of a Heat Exchanger with Offset-Strip Fins, *Int. J. Heat Mass Transfer*, vol. 54, pp. 2073–2079, 2011.
20. K. Park, D.-H. Choi, and K.-S. Lee, Numerical Shape Optimization for High Performance of a Heat Sink with Pin-Fins, *Numer. Heat Transfer A*, vol. 46, pp. 909–927, 2004.
21. P. Li and K.-Y. Kim, Multiobjective Optimization of Staggered Elliptical Pin-Fin Arrays, *Numer. Heat Transfer A*, vol. 53, pp. 418–431, 2008.
22. B. Kundu, A New Methodology for Determination of an Optimum Fin Shape under Dehumidifying Conditions, *Int. J. Refrigeration*, vol. 33, pp. 1105–1117, 2010.
23. M. Molki and A. Hashemi-Esfahanian, Turbulent Convective Mass Transfer Downstream of a Perforated Baffle Blockage, *Int. J. Heat Fluid Flow*, vol. 13, pp. 116–123, 1992.
24. B. Sahin and A. Demir, Performance Analysis of a Heat Exchanger Having Perforated Square Fins, *Appl. Therm. Eng.*, vol. 28, pp. 621–632, 2008.
25. O. N. Sara, T. Pekdemir, S. Yapici, and M. Yilmaz, Heat-Transfer Enhancement in a Channel Flow with Perforated Rectangular Blocks, *Int. J. Heat Fluid Flow*, vol. 22, pp. 509–518, 2001.

26. E. Dorignac, J.-J. Vullierme, M. Broussely, C. Foulon, and M. Mokkadem, Experimental Heat Transfer on the Windward Surface of a Perforated Flat Plate, *Int. J. Therm. Sci.*, vol. 44, pp. 885–893, 2005.
27. M. Yaghoubi, M. R. Shaeri, and K. Jafarpur, Three-Dimensional Numerical Laminar Convection Heat Transfer Around Lateral Perforated Fins, *Computational Therm. Sci.*, vol. 1, pp. 323–340, 2009.
28. E. Velayati and M. Yaghoubi, Numerical Study of Convective Heat Transfer from an Array of Parallel Bluff Plates, *Int. J. Heat Fluid Flow*, vol. 26, pp. 80–91, 2005.
29. C. W. Leung and S. D. Probert, Heat-Exchanger Performance: Effect of Orientation, *Appl. Energy*, vol. 33, pp. 235–252, 1989.
30. M. Yaghoubi and E. Velayati, Undeveloped Convective Heat Transfer from an Array of Cubes in Cross-Stream Direction, *Int. J. Therm. Sci.*, vol. 44, pp. 756–765, 2005.
31. M. Hadavand and M. Yaghoubi, Thermal Behavior of Curved Roof Buildings Exposed to Solar Radiation and Wind Flow for Various Orientations, *Appl. Energy*, vol. 85, pp. 663–679, 2008.
32. M. R. Khosravi Nikou and M. R. Ehsani, Turbulence Models Application on CFD Simulation of Hydrodynamics, Heat and Mass Transfer in a Structured Packing, *Int. Comm. Heat Mass Transfer*, vol. 35, pp. 1211–1219, 2008.
33. S. Eiamsa-ard and P. Promvonge, Numerical Study on Heat Transfer of Turbulent Channel Flow over Periodic Grooves, *Int. Comm. Heat Mass Transfer*, vol. 35, pp. 844–852, 2008.
34. V. Yakhot, S. A. Orszag, S. Thangam, T. B. Gatski, and C. G. Speziale, Development of Turbulence Models for Shear Flows by a Double Expansion Technique, *Physics of Fluids A*, vol. 4, pp. 1510–1520, 1992.
35. S. V. Patankar, *Numerical Heat Transfer and Fluid Flow*, Hemisphere, Washington, D.C., 1980.
36. H. Nakamura, T. Igarashi, and T. Tsutsui, Local Heat Transfer Around a Wall-Mounted Cube in the Turbulent Boundary Layer, *Int. J. Heat Mass Transfer*, vol. 44, pp. 3385–3395, 2001.
37. F. P. Incropera and D. P. DeWitt, *Introduction to Heat Transfer*, 3rd ed., John Wiley & Sons, Inc., 1996.